Locking-free higher-order energy-momentum schemes for thermo-viscoelastic fiber-reinforced materials derived by the principle of virtual power

Michael Groß, Julian Dietzsch & Chris Röbiger

Professorship of Applied Mechanics and Dynamics
Department of Mechanical Engineering

ICNAAM 2018 – MS 79 September 14, 2018

The Third Symposium on Border Zones between Experimental and Numerical Application including Solution Approaches by Extensions of Standard Numerical Methods

Acknowledgments: This research is provided by DFG under the grant GR 3297/4-1

Motivation, goals and strategy

Motivation: New simulation methods for fiber-reinforced materials

1. Energy-momentum schemes and locking-free FE methods are well-known algorithms
2. Problem: usually developed separately without a 'smart interface' between both
3. Idea: appropriate discrete variational principles can serve as such a 'smart interface'

Goal 1: Locking-free FE methods within energy-momentum schemes

Locking in volume elements

Simo, Taylor, Pister [1985]
Simo, Armero, Taylor [1993]
Kasper, Taylor [2000, 2004]
Schröder et al. [2011, 2016]

Energy-momentum schemes

Simo, Tarnow [1992]
Betsch, Steinmann [2000]
Noels, Stainier et al. [2004]
Romero [2010] ...

Locking-free energy-momentum schemes

Kuhl, Ramm [2000] Miehe, Schröder [2001] ...
Sansour et al. [2002] Armero [2008] Betsch et al. [2018]

Goal 2: volumetric locking in matrix & line locking in fibers

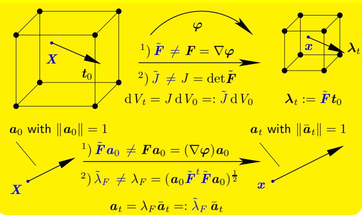

Strategy: Hu-Washizu functionals in the principle of virtual power

1. We design mixed variational principles which avoid static E.-L. equations
2. We derive energy-momentum schemes as discrete Euler-Lagrange equations

Hu-Washizu method and virtual power principle

Principle of virtual work / Hamilton's principle (Simo, Taylor, Pister [1985])

1. Internal energy functional

$$\mathit{\Pi}_{\mathrm{STP}}(\boldsymbol{\varphi},\tilde{J},p) := \int_{\mathscr{B}_0} \Psi^{\mathrm{iso}}(\boldsymbol{\varphi})\,\mathrm{d}V + \int_{\mathscr{B}_0} \Psi^{\mathrm{vol}}(\tilde{J})\,\mathrm{d}V - \int_{\mathscr{B}_0} p\,[\tilde{J} - \det(\nabla\boldsymbol{\varphi})]\,\mathrm{d}V$$

2. Euler-Lagrange equations for $\tilde{J}$ and $\boldsymbol{\varphi}$

$$\tilde{J} = \det(\nabla\boldsymbol{\varphi}) \qquad \rho_0\,\ddot{\boldsymbol{\varphi}} = \mathrm{Div}\left[2\,\nabla\boldsymbol{\varphi}\,\frac{\partial\Psi^{\mathrm{iso}}}{\partial\boldsymbol{C}} + p\,\mathrm{cof}(\nabla\boldsymbol{\varphi})\right] \quad \text{with} \quad \boldsymbol{C} = \boldsymbol{F}^t\boldsymbol{F}$$

Energy-momentum time integration (cf. Betsch & Steinmann [2002], Armero [2008])

1. Preservation of balance law of total energy $H := T(\dot{\boldsymbol{\varphi}}) + \Psi^{\mathrm{iso}}(\boldsymbol{\varphi}) + \Psi^{\mathrm{vol}}(\tilde{J})$

$$\mathcal{H}_{t_{n+1}} - \mathcal{H}_{t_n} = \int_{t_n}^{t_{n+1}}\int_{\mathcal{B}_0}\left[\frac{\partial H}{\partial\dot{\boldsymbol{\varphi}}}\cdot\ddot{\boldsymbol{\varphi}} + \frac{\partial H}{\partial\boldsymbol{\varphi}}\cdot\dot{\boldsymbol{\varphi}} + \frac{\partial H}{\partial\tilde{J}}\,\dot{\tilde{J}}\right]\mathrm{d}V\mathrm{d}t$$

2. Time evolution of volume dilatation $\tilde{J}$

$$\int_{t_n}^{t_{n+1}}\int_{\mathcal{B}_0}\delta p\,\dot{G}\,\mathrm{d}t = 0 \quad \text{with} \quad G(\boldsymbol{\varphi},\tilde{J}) := \tilde{J} - \det(\nabla\boldsymbol{\varphi})$$

Principle of virtual power (cf. Schröder & Kuhl [2015])

$$\int_{t_n}^{t_{n+1}}\delta_*\dot{\mathcal{H}}(\dot{\boldsymbol{\varphi}},\dot{\tilde{J}},p)\,\mathrm{d}t = 0 \quad \text{with} \quad \mathcal{H} := \frac{1}{2}\int_{\mathcal{B}_0}\rho_0\,\dot{\boldsymbol{\varphi}}\cdot\dot{\boldsymbol{\varphi}}\,\mathrm{d}V + \mathit{\Pi}_{\mathrm{STP}}(\boldsymbol{\varphi},\tilde{J},p)$$

Continuum model of a fiber-reinforced body (I)

Transversely isotropic material in non-isothermal motions

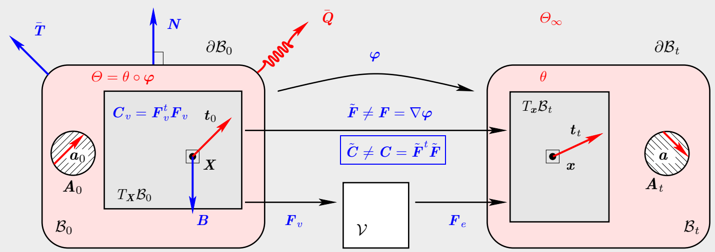

Deformation of fibers and matrix (cf. Klinkel, Sansour & Wagner [2005])

1. Deformation of the fibers

$$F_F := a_t \otimes a_0 = \tilde{F} A_0 \qquad A_0 := a_0 \otimes a_0 \qquad C_F := F_F^t F_F := C_F A_0$$

2. Fiber and volume dilatation

$$\tilde{C}_F \neq C_F := \tilde{C} : A_0 \qquad \tilde{C}_V \neq C_V := [\det(\tilde{C})]^{\frac{1}{n_{\mathrm{dim}}}}$$

3. Isotropic viscoelastic matrix

$$F = F_e F_v \qquad C_v = F_v^T F_v \qquad \rightsquigarrow \text{symmetric internal variable}$$

Continuum model of a fiber-reinforced body (II)

Thermo-viscoelastic free energy

1. Hyperelastic strain energy

$$\Psi^{\text{ela}}(\tilde{\boldsymbol{C}}, \tilde{C}_V, \tilde{C}_F; \boldsymbol{A}_0) = \hat{\Psi}^{\text{iso}}_M(I_1^{\tilde{C}}, I_2^{\tilde{C}}, I_3^{\tilde{C}}, I_4) + \hat{\Psi}^{\text{vol}}_M(\tilde{C}_V) + \hat{\Psi}^{\text{ela}}_F(\tilde{C}_F)$$

2. Thermoelastic free energy

$$\begin{aligned}\Psi^{\text{the}}(\Theta, \tilde{C}_V, \tilde{C}_F) = \hat{\Psi}^{\text{cap}}(\Theta) &- 2\sqrt{\tilde{C}_V{}^{2-n_{\text{dim}}}}\, \beta_M\, [\Theta - \Theta_\infty]\, \mathrm{D}\hat{\Psi}^{\text{vol}}_M(\tilde{C}_V) \\ &- 2\sqrt{\tilde{C}_F^{2-1}}\, \beta_F\, [\Theta - \Theta_\infty]\, \mathrm{D}\hat{\Psi}^{\text{ela}}_F(\tilde{C}_F)\end{aligned}$$

3. Viscoelastic free energy

$$\Psi^{\text{vis}}_M(\boldsymbol{\Lambda}) = \hat{\Psi}^{\text{ela}}_M(I_1^{\Lambda}, I_2^{\Lambda}, I_3^{\Lambda}) \qquad \boldsymbol{\Lambda} = \tilde{\boldsymbol{C}}\, \boldsymbol{C}_v^{-1} \qquad \boldsymbol{C}_e = \boldsymbol{F}_e^T \boldsymbol{F}_e$$

Non-equilibrium and total stress (cf. Reese [2001])

1. Viscous evolution equation and non-equilibrium stress tensor

$$\boxed{\boldsymbol{Y} = \boldsymbol{\Sigma}_v} \qquad \boldsymbol{Y} := -\frac{\partial \Psi^{\text{vis}}_M}{\partial \boldsymbol{C}_v} \qquad D^{\text{int}} := \dot{\boldsymbol{C}}_v : \boldsymbol{\Sigma}_v = \dot{\boldsymbol{C}}_v : \mathbb{V}(\boldsymbol{C}_v) : \dot{\boldsymbol{C}}_v \geq 0$$

$$\mathbb{V}(\boldsymbol{C}_v) = \frac{1}{4}\left[V_{\text{vol}} - \frac{V_{\text{dev}}}{n_{\text{dim}}}\right] \boldsymbol{C}_v^{-1} \otimes \boldsymbol{C}_v^{-1} + \frac{V_{\text{dev}}}{4}\, \mathbb{I}^{\text{sym}} : \boldsymbol{C}_v^{-1} \otimes \boldsymbol{C}_v^{-1}$$

2. Total second Piola-Kirchhoff stress tensor

$$\boldsymbol{S} := \boldsymbol{S}^{\text{iso}}_M + \boldsymbol{S}^{\text{vis}}_M + S_V\, \boldsymbol{A}^{\text{vol}} + S_F\, \boldsymbol{A}_0 \qquad \boldsymbol{A}^{\text{vol}} := \frac{1}{n_{\text{dim}}} \det(\tilde{\boldsymbol{C}})^{\frac{1}{n_{\text{dim}}}}\, \tilde{\boldsymbol{C}}^{-1}$$

Basis of the principle of virtual power (I)

Locking-free higher-order energy-momentum schemes for thermo-viscoelastic fiber-reinforced materials derived by the principle of virtual power

Michael Groß, Julian Dietzsch & Chris Röbiger

Introduction
Variational setting
Continuum model
Variational principle
Discrete setting
Time discretization
Space discretization
Example: H8 mesh
Numerical studies
Numerical example
Configuration and solution
Comparison
Summary

Total energy balance law in functional form with independent fields

$$\dot{\mathcal{H}}(\underbrace{\dot{\boldsymbol{\varphi}}, \dot{\boldsymbol{v}}, \dot{\boldsymbol{p}}, \dot{\boldsymbol{C}}_v, \dot{\Theta}, \dot{\eta}, \dot{\tilde{\boldsymbol{F}}}, \dot{\tilde{\boldsymbol{C}}}, \dot{\tilde{C}}_V, \dot{\tilde{C}}_F}_{\text{temporally continuous}}, \underbrace{\underbrace{\tilde{\Theta}, \boldsymbol{P}, \boldsymbol{S}, S_V, S_F, \boldsymbol{R}, h, \lambda}; \underbrace{\tilde{\boldsymbol{S}}, \tilde{S}_V, \tilde{S}_F}}_{\text{temporally discontinuous parameters}}) = 0 \quad \text{with} \quad \dot{\mathcal{H}} = \dot{\mathcal{T}} + \dot{\Pi}^{\text{int}} + \dot{\Pi}^{\text{ext}}$$

External power functional

$$D^{\text{cdu}} = -\nabla(\ln \Theta) \cdot \boldsymbol{Q}$$

$$\begin{aligned}
\dot{\Pi}^{\text{ext}} := & \int_{\mathscr{B}_0} \frac{1}{2}\, \tilde{\boldsymbol{S}} : \dot{\tilde{\boldsymbol{C}}} \,\mathrm{d}V + \int_{\mathscr{B}_0} \frac{1}{2}\, \tilde{S}_V\, \dot{\tilde{C}}_V \,\mathrm{d}V + \int_{\mathscr{B}_0} \frac{1}{2}\, \tilde{S}_F\, \dot{\tilde{C}}_F \,\mathrm{d}V \\
& - \int_{\mathscr{B}_0} \rho_0 \boldsymbol{B} \cdot \dot{\boldsymbol{\varphi}} \,\mathrm{d}V - \int_{\partial_T \mathscr{B}_0} \bar{\boldsymbol{T}} \cdot \dot{\boldsymbol{\varphi}} \,\mathrm{d}A + \int_{\partial_Q \mathscr{B}_0} \frac{\tilde{\Theta}}{\Theta}\, \bar{Q} \,\mathrm{d}A \\
& + \int_{\mathscr{B}_0} \frac{1}{\Theta} \nabla \tilde{\Theta} \cdot \boldsymbol{Q} \,\mathrm{d}V + \int_{\mathscr{B}_0} \frac{\tilde{\Theta}}{\Theta} \left(D^{\text{cdu}} + D^{\text{int}}\right) \mathrm{d}V + \int_{\mathscr{B}_0} \dot{\boldsymbol{C}}_v : \boldsymbol{\Sigma}_v \,\mathrm{d}V \\
& + \int_{\partial_\Theta \mathscr{B}_0} \lambda \left[\tilde{\Theta} - \Theta_\infty\right] \mathrm{d}A - \int_{\partial_{\dot{\Theta}} \mathscr{B}_0} h \left[\dot{\Theta} - \dot{\bar{\Theta}}\right] \mathrm{d}A - \int_{\partial_\varphi \mathscr{B}_0} \boldsymbol{R} \cdot \left[\dot{\boldsymbol{\varphi}} - \dot{\bar{\boldsymbol{\varphi}}}\right] \mathrm{d}A
\end{aligned}$$

Kinetic energy in Hu-Washizu form

$$T(\boldsymbol{v}) = \frac{\rho_0}{2}\, \boldsymbol{v} \cdot \boldsymbol{v} \qquad \mathcal{T} := \int_{\mathscr{B}_0} T(\boldsymbol{v}) \,\mathrm{d}V - \int_{\mathscr{B}_0} [\boldsymbol{v} - \dot{\boldsymbol{\varphi}}] \cdot \boldsymbol{p} \,\mathrm{d}V$$

Kinetic power functional (with independent time rate fields)

$$\dot{\mathcal{T}}(\dot{\boldsymbol{\varphi}}, \dot{\boldsymbol{v}}, \dot{\boldsymbol{p}}) := \int_{\mathscr{B}_0} \left[\frac{\partial T}{\partial \boldsymbol{v}} - \boldsymbol{p}\right] \cdot \dot{\boldsymbol{v}} \,\mathrm{d}V - \int_{\mathscr{B}_0} \dot{\boldsymbol{p}} \cdot [\boldsymbol{v} - \dot{\boldsymbol{\varphi}}] \mathrm{d}V + \int_{\mathscr{B}_0} \boldsymbol{p} \cdot \ddot{\boldsymbol{\varphi}} \,\mathrm{d}V$$

Basis of the principle of virtual power (II)

Fourier's law of transversely isotropic heat conduction

Al-Kinani [2014]

$$\boldsymbol{q} := -\boldsymbol{\kappa}\boldsymbol{F}^{-T}\nabla\Theta \qquad \boldsymbol{\kappa} := k\,\boldsymbol{I} + \frac{k_F - k}{\|\boldsymbol{a}\|^2}\boldsymbol{a}\otimes\boldsymbol{a} \qquad \boldsymbol{\kappa}_0 := k_0\,\boldsymbol{C}^{-1} + \frac{k_{F_0} - k_0}{C_F}\boldsymbol{A}_0 \qquad \boldsymbol{Q} := -\boldsymbol{\kappa_0}\,\nabla\Theta$$

Internal energy

$$\begin{aligned}\Pi^{\text{int}} :=\ & \int_{\mathscr{B}_0}\hat{\Psi}_M(\boldsymbol{C}_v,\tilde{\boldsymbol{C}},\tilde{C}_V,\Theta;\boldsymbol{A}_0)\,\mathrm{d}V + \int_{\mathscr{B}_0}\hat{\Psi}_F(\tilde{C}_F,\Theta)\,\mathrm{d}V - \int_{\mathscr{B}_0}\eta\,[\tilde{\Theta}-\Theta]\,\mathrm{d}V \\ & - \int_{\mathscr{B}_0}\boldsymbol{P} : [\tilde{\boldsymbol{F}} - \nabla\boldsymbol{\varphi}]\,\mathrm{d}V - \frac{1}{2}\int_{\mathscr{B}_0}\boldsymbol{S} : \left[\tilde{\boldsymbol{C}} - \tilde{\boldsymbol{F}}^t\tilde{\boldsymbol{F}}\right]\mathrm{d}V \\ & - \frac{1}{2}\int_{\mathscr{B}_0}S_F\,[\tilde{C}_F - \tilde{\boldsymbol{C}} : \boldsymbol{A}_0]\,\mathrm{d}V - \frac{1}{2}\int_{\mathscr{B}_0}S_V\left[\tilde{C}_V - \det(\tilde{\boldsymbol{C}})^{\frac{1}{n_{\text{dim}}}}\right]\mathrm{d}V\end{aligned}$$

Internal power functional

$$\begin{aligned}\dot{\Pi}^{\text{int}} :=\ & \frac{1}{2}\int_{\mathscr{B}_0}\left\{\left[2\,\frac{\partial\hat{\Psi}_M}{\partial\tilde{\boldsymbol{C}}} + S_V\,\boldsymbol{A}^{\text{vol}} + S_F\,\boldsymbol{A}_0 - \boldsymbol{S}\right] : \dot{\tilde{\boldsymbol{C}}} + \left[2\,\frac{\partial\hat{\Psi}_M}{\partial\tilde{C}_V} - S_V\right] : \dot{\tilde{C}}_V\right\}\mathrm{d}V - \int_{\mathscr{B}_0}\dot{\eta}\,[\tilde{\Theta}-\Theta]\,\mathrm{d}V \\ & + \frac{1}{2}\int_{\mathscr{B}_0}\left[2\,\frac{\partial\hat{\Psi}_F}{\partial\tilde{C}_F} - S_F\right] : \dot{\tilde{C}}_F\,\mathrm{d}V + \int_{\mathscr{B}_0}\left\{[\tilde{\boldsymbol{F}}\boldsymbol{S} - \boldsymbol{P}] : \dot{\tilde{\boldsymbol{F}}} + \frac{\partial\hat{\Psi}_M}{\partial\boldsymbol{C}_v} : \dot{\boldsymbol{C}}_v\right\}\mathrm{d}V + \int_{\mathscr{B}_0}\left[\eta + \frac{\partial\Psi}{\partial\Theta}\right]\dot{\Theta}\,\mathrm{d}V \\ & + \int_{\mathscr{B}_0}\boldsymbol{P} : \nabla\dot{\boldsymbol{\varphi}}\,\mathrm{d}V - \int_{\mathscr{B}_0}\dot{\boldsymbol{P}} : [\tilde{\boldsymbol{F}} - \nabla\boldsymbol{\varphi}]\,\mathrm{d}V - \frac{1}{2}\int_{\mathscr{B}_0}\dot{\boldsymbol{S}} : \left[\tilde{\boldsymbol{C}} - \tilde{\boldsymbol{F}}^t\tilde{\boldsymbol{F}}\right]\mathrm{d}V + \int_{\mathscr{B}_0}\dot{\tilde{\Theta}}\,\eta\,\mathrm{d}V \\ & - \frac{1}{2}\int_{\mathscr{B}_0}\dot{S}_V : \left[\tilde{C}_V - \det(\tilde{\boldsymbol{C}})^{\frac{1}{n_{\text{dim}}}}\right]\mathrm{d}V - \frac{1}{2}\int_{\mathscr{B}_0}\dot{S}_F : [\tilde{C}_F - \tilde{\boldsymbol{C}} : \boldsymbol{A}_0]\,\mathrm{d}V\end{aligned}$$

Principle of virtual power (cf. Schröder & Kuhl [2015], Klinkel & Wagner [1997], Hackl [1997])

Principle of virtual power

$$\delta_*\dot{\mathcal{H}}(\dot{\boldsymbol{\varphi}},\dot{\boldsymbol{v}},\dot{\boldsymbol{p}},\dot{\boldsymbol{C}}_v,\dot{\Theta},\dot{\eta},\dot{\tilde{\boldsymbol{F}}},\dot{\tilde{\boldsymbol{C}}},\dot{\tilde{C}}_V,\dot{\tilde{C}}_F,\tilde{\Theta},\boldsymbol{P},\boldsymbol{S},S_V,S_F,\boldsymbol{R},h,\lambda;\tilde{\boldsymbol{S}},\tilde{S}_V,\tilde{S}_F)=0 \quad \text{with} \quad \dot{\mathcal{H}}=\dot{\mathcal{T}}+\dot{\Pi}^{\text{int}}+\dot{\Pi}^{\text{ext}}$$

Virtual kinetic power

$$\delta_*\dot{\mathcal{T}}(\dot{\boldsymbol{u}},\dot{\boldsymbol{v}},\dot{\boldsymbol{p}}):=\int_{\mathscr{B}_0}\left[\frac{\partial T}{\partial\boldsymbol{v}}-\boldsymbol{p}\right]\cdot\delta_*\dot{\boldsymbol{v}}\,\mathrm{d}V-\int_{\mathscr{B}_0}\delta_*\dot{\boldsymbol{p}}\cdot[\boldsymbol{v}-\dot{\boldsymbol{\varphi}}]\,\mathrm{d}V+\int_{\mathscr{B}_0}\dot{\boldsymbol{p}}\cdot\delta_*\dot{\boldsymbol{\varphi}}\,\mathrm{d}V$$

Virtual external power

$$\begin{aligned}\delta_*\dot{\Pi}^{\text{ext}}:=&-\int_{\mathscr{B}_0}\rho_0\boldsymbol{B}\cdot\delta_*\dot{\boldsymbol{\varphi}}\,\mathrm{d}V-\int_{\partial_T\mathscr{B}_0}\bar{\boldsymbol{T}}\cdot\delta_*\dot{\boldsymbol{\varphi}}\,\mathrm{d}A-\int_{\partial_\varphi\mathscr{B}_0}\delta_*\boldsymbol{R}\cdot[\dot{\boldsymbol{\varphi}}-\dot{\bar{\boldsymbol{\varphi}}}]\,\mathrm{d}A-\int_{\partial_\varphi\mathscr{B}_0}\boldsymbol{R}\cdot\delta_*\dot{\boldsymbol{\varphi}}\\&+\int_{\mathscr{B}_0}\frac{1}{\Theta}\nabla(\delta_*\tilde{\Theta})\cdot\boldsymbol{Q}\,\mathrm{d}V+\int_{\mathscr{B}_0}\delta_*\tilde{\Theta}\,\frac{D^{\text{cdu}}+D^{\text{int}}}{\Theta}\,\mathrm{d}V+\int_{\mathscr{B}_0}\delta_*\dot{\boldsymbol{C}}_v:\boldsymbol{\Sigma}_v\,\mathrm{d}V+\int_{\partial_\Theta\mathscr{B}_0}\lambda\,\delta_*\tilde{\Theta}\,\mathrm{d}A\\&+\int_{\partial_Q\mathscr{B}_0}\frac{\delta_*\tilde{\Theta}}{\Theta}\,\bar{Q}\,\mathrm{d}A+\int_{\partial_\Theta\mathscr{B}_0}\delta_*\lambda\left[\tilde{\Theta}-\Theta_\infty\right]\mathrm{d}A-\int_{\partial_{\dot{\Theta}}\mathscr{B}_0}\delta_*h\left[\dot{\Theta}-\dot{\bar{\Theta}}\right]\mathrm{d}A-\int_{\partial_{\dot{\Theta}}\mathscr{B}_0}\delta_*\dot{\Theta}\,h\,\mathrm{d}A\\&+\int_{\mathscr{B}_0}\frac{1}{2}\,\tilde{\boldsymbol{S}}:\delta_*\dot{\tilde{\boldsymbol{C}}}\,\mathrm{d}V+\int_{\mathscr{B}_0}\frac{1}{2}\,\tilde{S}_V\,\delta_*\dot{\tilde{C}}_V\,\mathrm{d}V+\int_{\mathscr{B}_0}\frac{1}{2}\,\tilde{S}_F\,\delta_*\dot{\tilde{C}}_F\,\mathrm{d}V\end{aligned}$$

Virtual internal power

$$\begin{aligned}\delta_*\dot{\Pi}^{\text{int}}:=&\ \frac{1}{2}\int_{\mathscr{B}_0}\left[2\,\frac{\partial\hat{\Psi}_M}{\partial\tilde{\boldsymbol{C}}}+S_V\,\boldsymbol{A}^{\text{vol}}+S_F\,\boldsymbol{A}_0-\boldsymbol{S}\right]:\delta_*\dot{\tilde{\boldsymbol{C}}}\,\mathrm{d}V-\int_{\mathscr{B}_0}\dot{\eta}\,\delta_*\tilde{\Theta}\,\mathrm{d}V+\int_{\mathscr{B}_0}\delta_*\dot{\boldsymbol{C}}_v:\frac{\partial\hat{\Psi}_M}{\partial\boldsymbol{C}_v}\,\mathrm{d}V\\&+\frac{1}{2}\int_{\mathscr{B}_0}\left[2\,\frac{\partial\hat{\Psi}_M}{\partial\tilde{C}_V}-S_V\right]:\delta_*\dot{\tilde{C}}_V\,\mathrm{d}V+\frac{1}{2}\int_{\mathscr{B}_0}\left[2\,\frac{\partial\hat{\Psi}_F}{\partial\tilde{C}_F}-S_F\right]:\delta_*\dot{\tilde{C}}_F\,\mathrm{d}V+\int_{\mathscr{B}_0}\nabla(\delta_*\dot{\boldsymbol{\varphi}}):\boldsymbol{P}\,\mathrm{d}V\\&-\frac{1}{2}\int_{\mathscr{B}_0}\left\{\left[\dot{\tilde{C}}_V-\dot{\tilde{\boldsymbol{C}}}:\boldsymbol{A}^{\text{vol}}\right]:\delta_*S_V-\left[\dot{\tilde{C}}_F-\dot{\tilde{\boldsymbol{C}}}:\boldsymbol{A}_0\right]:\delta_*S_F\right\}\mathrm{d}V+\int_{\mathscr{B}_0}\delta_*\dot{\tilde{\boldsymbol{F}}}:\left[\tilde{\boldsymbol{F}}\boldsymbol{S}-\boldsymbol{P}\right]\mathrm{d}V\\&-\frac{1}{2}\int_{\mathscr{B}_0}\frac{\mathrm{d}}{\mathrm{d}t}\left[\tilde{\boldsymbol{C}}-\tilde{\boldsymbol{F}}^t\tilde{\boldsymbol{F}}\right]:\delta_*\boldsymbol{S}\,\mathrm{d}V+\int_{\mathscr{B}_0}\left\{\left[\frac{\partial\Psi}{\partial\Theta}+\eta\right]\delta_*\dot{\Theta}-\left[\tilde{\Theta}-\Theta\right]\delta_*\dot{\eta}-\delta_*\boldsymbol{P}:\left[\dot{\tilde{\boldsymbol{F}}}-\nabla\dot{\boldsymbol{\varphi}}\right]\right\}\mathrm{d}V\end{aligned}$$

Design of the mixed time discretization

Schematic process of the energy-momentum scheme design (cf. Yavari [2008])

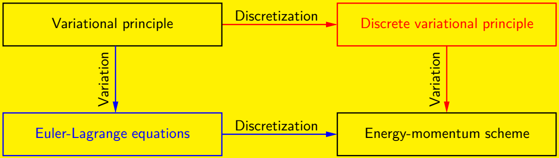

Different time scales in the time integration (cf. Kassiotis et al. [2009])

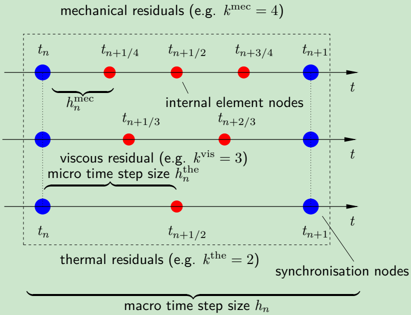

k	$M_I(\alpha)$	α_I	$\tilde{M}_J(\alpha)$	$\tilde{\alpha}_J$
1	$1-\alpha$	0	1	1
	α	1		
2	$(2\alpha-1)(\alpha-1)$	0	$1-\alpha$	0
	$-4\alpha\,(\alpha-1)$	$\frac{1}{2}$	α	1
	$(2\alpha-1)\,\alpha$	1		
3	$-\frac{9}{2}\,(\alpha-\frac{1}{3})(\alpha-\frac{2}{3})(\alpha-1)$	0	$(2\alpha-1)(\alpha-1)$	0
	$\frac{27}{2}\,(\alpha-\frac{2}{3})(\alpha-1)\,\alpha$	$\frac{1}{3}$	$-4\alpha\,(\alpha-1)$	$\frac{1}{2}$
	$-\frac{27}{2}\,(\alpha-\frac{1}{3})(\alpha-1)\,\alpha$	$\frac{2}{3}$	$(2\alpha-1)\,\alpha$	1
	$\frac{9}{2}\,(\alpha-\frac{1}{3})(\alpha-\frac{2}{3})\,\alpha$	1		
4	$\frac{32}{3}\,(\alpha-\frac{1}{4})(\alpha-\frac{1}{2})(\alpha-\frac{3}{4})(\alpha-1)$	0	$-\frac{9}{2}\,(\alpha-\frac{1}{3})(\alpha-\frac{2}{3})(\alpha-1)$	0
	$-\frac{128}{3}\,(\alpha-\frac{1}{2})(\alpha-\frac{3}{4})(\alpha-1)\alpha$	$\frac{1}{4}$	$\frac{27}{2}\,(\alpha-\frac{2}{3})(\alpha-1)\,\alpha$	$\frac{1}{3}$
	$64\,(\alpha-\frac{1}{4})(\alpha-\frac{3}{4})(\alpha-1)\alpha$	$\frac{1}{2}$	$-\frac{27}{2}\,(\alpha-\frac{1}{3})(\alpha-1)\,\alpha$	$\frac{2}{3}$
	$-\frac{128}{3}\,(\alpha-\frac{1}{4})(\alpha-\frac{1}{2})(\alpha-1)\alpha$	$\frac{3}{4}$	$\frac{9}{2}\,(\alpha-\frac{1}{3})(\alpha-\frac{2}{3})\,\alpha$	1
	$\frac{32}{3}\,(\alpha-\frac{1}{4})(\alpha-\frac{1}{2})(\alpha-\frac{3}{4})\alpha$	1		

$$\phi^n(\alpha) := \sum_{I=1}^{k^{\mathrm{mec}}+1} M_I^{\mathrm{mec}}(\alpha)\,\phi_I$$

$$\alpha(t) := \frac{t-t_n}{h_n} \in [0,1]$$

Locking-free higher-order energy-momentum schemes for thermo-viscoelastic fiber-reinforced materials derived by the principle of virtual power

Michael Groß, Julian Dietzsch & Chris Röbiger

Design of the mixed space discretization

Analytical static condensation of mixed fields

1. First Piola-Kirchhoff stress tensor $\boldsymbol{P}$ is condensed out $\rightsquigarrow$ only a new 'B-matrix'
2. $\tilde{\boldsymbol{F}}$, $\tilde{C}_F$, $\tilde{C}_V$ are temporally continuous fields $\rightsquigarrow$ initial value is taken into account

Space approximation of mixed fields

$\deg[X]$ = degree of spatial shape functions of X

1. $\underbrace{\deg[\dot{\boldsymbol{\varphi}}, \dot{\boldsymbol{v}}, \dot{\boldsymbol{p}}, \dot{\Theta}, \dot{\eta}, \tilde{\Theta}]}_{\text{spatially continuous}} \geq \underbrace{\deg[\dot{\tilde{\boldsymbol{F}}}, \boldsymbol{P}] \geq \deg[\dot{C}_V, \dot{C}_F, S_V, S_F]}_{\text{spatially discontinuous}}$ (motivated by Q1P0, Q2P1 etc.)
2. Evaluation of $\tilde{\boldsymbol{C}}$, $\boldsymbol{C}_v$ and $\boldsymbol{S}$ at spatial quadrature points

Strategy for choosing shape functions of mixed fields

(cf. Mahnken et al. [2008])

1. Choose $\deg[\dot{\boldsymbol{\varphi}}, \dot{\boldsymbol{v}}, \dot{\boldsymbol{p}}, \dot{\Theta}, \dot{\eta}, \tilde{\Theta}]$ and they kind of shape functions (hexahedral or tetrahedral)
2. Determine independent spatial shape functions N_A, $\tilde{N}_B^{\mathrm{def}}$, $\tilde{N}_C^{\mathrm{str}}$, which fulfill the condition
$$\deg[\dot{\boldsymbol{\varphi}}, \dot{\boldsymbol{v}}, \dot{\boldsymbol{p}}, \dot{\Theta}, \tilde{\Theta}, \dot{\eta}] = \deg[\dot{\tilde{\boldsymbol{F}}}, \boldsymbol{P}] + 1 = \deg[\dot{C}_V, \dot{C}_F, S_V, S_F] + 2$$
3. Extend the shape functions $\tilde{N}_B^{\mathrm{def}}$, $\tilde{N}_C^{\mathrm{str}}$ by area bubbles in order to include each monomial and fulfill the completeness conditions
$$\sum_{B=1}^{\tilde{n}_{\mathrm{def}}} \tilde{N}_B^{\mathrm{def}} = 1 \qquad \sum_{C=1}^{\tilde{n}_{\mathrm{str}}} \tilde{N}_C^{\mathrm{str}} = 1$$

Michael Groß, Julian Dietzsch & Chris Röbiger

Example: Mesh of 8-node hexahedral elements

Motivation: time discretization (cf. Betsch & Steinmann [2002])

1. Example: Trial functions for the deformation φ of degree $k=2$, given by

$$M_1(\alpha) = (2\,\alpha - 1)(\alpha - 1) \qquad M_2(\alpha) = -4\,\alpha\,(\alpha - 1) \qquad M_3(\alpha) = \alpha\,(2\,\alpha - 1)$$

demands for the variation $\delta\varphi$ test functions of degree $k-1=1$ of the form

$$\tilde{M}_1(\alpha) = 1 - \alpha \qquad \tilde{M}_2(\alpha) = \alpha$$

2. Proof: The time functions $M_1'(\alpha) = 4\,\alpha - 3$, $M_2'(\alpha) = 4 - 8\,\alpha$ and $M_3'(\alpha) = 4\,\alpha - 1$ are not independent, which means

$$\sum_{i=1}^{k+1} a_i\, M_i'(\alpha) = 0 \qquad \text{leads to } a_i = \lambda_1 \in \mathbb{R} \text{ with } p = 1 \text{ parameter}$$

Therefore, only $k-p=2$ functions $\tilde{M}_j$ are independent, and (i) gives the identity

$$\sum_{i=1}^{k+1} M_i'(\alpha)\, z_i = \sum_{j=1}^{k} \tilde{M}_j\, \tilde{z}_j \qquad \text{and (ii) includes the required monomials} \qquad 1,\ \alpha$$

Application: space discretization with 8-node hexahedrons (cf. Armero [2008])

1. The 8 shape functions N_A have 4 independent derivatives, which leads to

$$\tilde{N}_1^{\text{def}} = 1 - \xi - \eta - \zeta \qquad \tilde{N}_2^{\text{def}} = \xi \qquad \tilde{N}_3^{\text{def}} = \eta \qquad \tilde{N}_4^{\text{def}} = \zeta$$

2. The 4 shape functions $\tilde{N}_B^{\text{def}}$ have 1 independent derivative $\tilde{N}^{\text{str}} = 1$.

3. Since the derivatives of N_A include the monomials $\xi\eta$, $\xi\zeta$ and $\eta\zeta$, we define

$$\tilde{N}_1^{\text{def}} := \tilde{N}_1^{\text{def}} - \xi\eta - \xi\zeta - \eta\zeta \qquad \tilde{N}_2^{\text{def}} := \tilde{N}_2^{\text{def}} + \eta\zeta \qquad \tilde{N}_3^{\text{def}} := \tilde{N}_3^{\text{def}} + \xi\zeta \qquad \tilde{N}_4^{\text{def}} := \tilde{N}_4^{\text{def}} + \xi\eta$$

Fiber-reinforced air beam with two cells

(Boundary and initial conditions; $k_{\text{mec}} = 1$, $k_{\text{the}} = 2$, $k_{\text{vis}} = 1$)

Boundary Status Monitor

(cf. Nguyen et al. [2015])

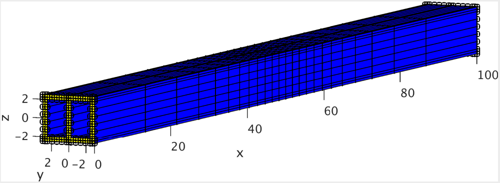

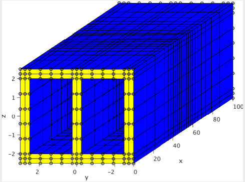

Dirichlet and Neumann boundary conditions

$\varphi_t^A = \boldsymbol{X}^A$ (circular markers) (clamped at both ends)

$\Theta_t^A = \Theta_\infty$ (blue patches) No thermal insulation $\bar{Q} := 0$

Transient pressure

(follower load in star markers)

$$f_p(t) := \hat{p}\,|\sin(\omega_{\text{load},\text{p}}\, t)|$$

Temperature profile (yellow patches) $f_L(t) := \sin(\omega_{\text{load}}\, t)$

$$f(t) = \begin{cases} (1.0\, f_L(t))^2 & \forall T_{\text{load}}(0.0 + c_{\text{load}}) < t \leq T_{\text{load}}(0.2 + c_{\text{load}}) \\ (1.2\, f_L(t))^2 & \forall T_{\text{load}}(0.2 + c_{\text{load}}) < t \leq T_{\text{load}}(0.4 + c_{\text{load}}) \\ (1.4\, f_L(t))^2 & \forall T_{\text{load}}(0.4 + c_{\text{load}}) < t \leq T_{\text{load}}(0.6 + c_{\text{load}}) \\ (1.2\, f_L(t))^2 & \forall T_{\text{load}}(0.6 + c_{\text{load}}) < t \leq T_{\text{load}}(0.8 + c_{\text{load}}) \\ (1.0\, f_L(t))^2 & \forall T_{\text{load}}(0.8 + c_{\text{load}}) < t \leq T_{\text{load}}(1.0 + c_{\text{load}}) \end{cases}$$

Initial conditions

(Ambient temp. $\Theta_\infty = 298.15$)

$$\boldsymbol{\varphi}_0^A = \boldsymbol{X}^A$$
$$\boldsymbol{v}_0^A = \boldsymbol{0}$$
$$\Theta_0^A = \Theta_\infty + 10$$

Fiber-reinforced air beam with two cells

(Parameters and fiber directions; $k_{\mathrm{mec}} = 1$, $k_{\mathrm{the}} = 2$, $k_{\mathrm{vis}} = 1$)

Michael Groß, Julian Dietzsch & Chris Röbiger

Simulation parameters $\Theta_\infty = 298.15$

Initial conditions	
Initial velocity:	$\boldsymbol{v}_0^A = \mathbf{0}$
Initial temperature:	$\Theta_0^A = \Theta_\infty + 10 = 308.15$
Boundary conditions	
Yellow patches in yz-plain (with circular markers):	x-dof, y-dof and z-dof fixed
Yellow patches:	$\Theta^A = \hat{\Theta}\, f(t)$
Blue patches:	$\Theta^A = \Theta_\infty$
Dirichlet loads	
Temperature profile: (yellow patches)	$f(t)$ with $\hat{\Theta} = 10$, $T_{\mathrm{load}} = 2.0$, $\omega_{\mathrm{load}} = 10\pi$
Neumann loads	
Pressure load: (blue patches with star markers)	$f_p(t)$ with $\hat{p} = 1 \cdot 10^5$, $T_{\mathrm{load,p}} = 2.0$, $\omega_{\mathrm{load,p}} = 10\pi$
Volume loads	
Standard gravity	$g = 9.81$ with $\boldsymbol{e}_g = -\boldsymbol{e}_z$

Material Status Monitor

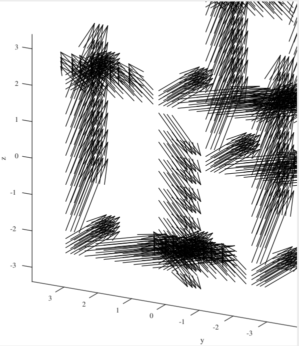

Material parameters

$\rho_0 = 1.120 \cdot 10^3$	$\kappa^{\mathrm{vol}} = 1.000 \cdot 10^7$	$\mu_{01} = 0.250 \cdot 10^4$
$\mu_{10} = 0.250 \cdot 10^7$	$\mu_{20} = 0.021 \cdot 10^7$	$Y_1 = 0.1631 \cdot 10^7$
$Y_2 = 0.6$	$\kappa_{\mathrm{ani}} = 0.250 \cdot 10^7$	$g_0 = 0.300 \cdot 10^7$
$g_c = 4$	$\beta_M = 20 \cdot 10^{-6}$	$c_{M_0} = 1539 \cdot 50\%$
$c_{M_1} = 0.00375$	$k = 0.2595$	$\beta_F = 206 \cdot 10^{-6}$
$c_{F_0} = 1539 \cdot 50\%$	$c_{F_1} = 0.00375$	$k_F = 200\, k$
$V_{\mathrm{dev}} = 10^3$	$V_{\mathrm{vol}} = 5 \cdot 10^3$	$\kappa_v^{\mathrm{vol}} = 1.000 \cdot 10^6$
$\mu_{01}^v = 0.250 \cdot 10^3$	$\mu_{10}^v = 0.250 \cdot 10^6$	$\mu_{20}^v = 0.021 \cdot 10^6$
$Y_1^v = 0.1631 \cdot 10^6$	$Y_2^v = 0.6$	

Fiber directions

Side walls	: $\boldsymbol{a}_0 = \sin\phi\, \boldsymbol{e}_x + \cos\phi\, \boldsymbol{e}_z$, $\phi = \frac{\pi}{4}$
Middle wall	: $\boldsymbol{a}_0 = \sin\phi\, \boldsymbol{e}_x + \cos\phi\, \boldsymbol{e}_z$, $\phi = \frac{3\pi}{4}$
Bottom left/ top right	: $\boldsymbol{a}_0 = \sin\phi\, \boldsymbol{e}_x + \cos\phi\, \boldsymbol{e}_y$, $\phi = \frac{3\pi}{4}$
Bottom right/ top left	: $\boldsymbol{a}_0 = \sin\phi\, \boldsymbol{e}_x + \cos\phi\, \boldsymbol{e}_y$, $\phi = \frac{\pi}{4}$
Chamber corners	: $\boldsymbol{a}_0 = \sin\phi\, \boldsymbol{e}_x + \cos\phi\, \boldsymbol{e}_y$, $\phi = \frac{\pi}{2}$

Fiber-reinforced air beam with two cells

(Free energy functions and loads; $k_{\mathrm{mec}} = 1$, $k_{\mathrm{the}} = 2$, $k_{\mathrm{vis}} = 1$)

Free energy

$(\boldsymbol{C}^{\mathrm{iso}} := [I_3^C]^{\frac{-1}{n_{\mathrm{dim}}}}\,\boldsymbol{C},\ \Theta_\infty = 298.15)$

Elastic free energy functions

$$
\begin{aligned}
\Psi_M^{\mathrm{ela}} &:= \mu_{10}\left[I_1(\boldsymbol{C}^{\mathrm{iso}}) - I_1(\boldsymbol{I})\right] \\
&\quad + \mu_{20}\left[I_1(\boldsymbol{C}^{\mathrm{iso}})) - I_1(\boldsymbol{I})\right]^2 \\
&\quad + \mu_{01}\left[I_2(\boldsymbol{C}^{\mathrm{iso}}) - I_2(\boldsymbol{I})\right] \\
&\quad + \frac{Y_1}{Y_2}\left\{1 - \exp\left[-Y_2\left(I_1(\boldsymbol{C}^{\mathrm{iso}}) - I_1(\boldsymbol{I})\right)\right]\right\} \\
&\quad + \frac{\kappa^{\mathrm{ani}}}{3}\left[\left(I_4(\boldsymbol{C}^{\mathrm{iso}})\right)^{3/2} + 3\left(I_4(\boldsymbol{C}^{\mathrm{iso}})\right)^{-1/2} - 4\right] \\
\Psi_M^{\mathrm{vol}} &:= \frac{\kappa^{\mathrm{vol}}}{50}\left[\left(\tilde{C}_V\right)^{5 n_{\mathrm{dim}}/2} + \left(\tilde{C}_V\right)^{-5 n_{\mathrm{dim}}/2} - 2\right] \\
\Psi_F^{\mathrm{ela}} &:= \frac{g_0}{(2\,g_c)}\left[\exp\left[g_c(\tilde{C}_F - 1)^2\right] - 1\right]
\end{aligned}
$$

Thermoelastic free energy function

$$
\begin{aligned}
\Psi^{\mathrm{cap}} &:= c_0\,(1 - \Theta_\infty\,c_1)\left[\Theta - \Theta_\infty - \Theta\,\ln\left(\frac{\Theta}{\Theta_\infty}\right)\right] \\
&\quad - \frac{1}{2}\,c_0\,c_1\,(\Theta - \Theta_\infty)^2 \\
\hat{\Psi}_M^{\mathrm{the}} &:= \hat{\Psi}_M^{\mathrm{cap}} - 2\sqrt{C_V^{2-n_{\mathrm{dim}}}}\,\beta_M\,(\Theta - \Theta_\infty)\,\mathrm{D}\hat{\Psi}_M^{\mathrm{vol}}(C_V) \\
\hat{\Psi}_F^{\mathrm{the}} &:= \hat{\Psi}_F^{\mathrm{cap}} - 2\sqrt{C_F}\,\beta_F\,(\Theta - \Theta_\infty)\,\mathrm{D}\hat{\Psi}_F^{\mathrm{ela}}(C_F)
\end{aligned}
$$

Viscoelastic free energy function

$$
\begin{aligned}
\Psi_M^{\mathrm{vis}} &:= \mu_{10}^v\left[I_1(\boldsymbol{\Lambda}^{\mathrm{iso}}) - I_1(\boldsymbol{I})\right] \\
&\quad + \mu_{20}^v\left[I_1(\boldsymbol{\Lambda}^{\mathrm{iso}})) - I_1(\boldsymbol{I})\right]^2 \\
&\quad + \mu_{01}^v\left[I_2(\boldsymbol{\Lambda}^{\mathrm{iso}}) - I_2(\boldsymbol{I})\right] \\
&\quad + \frac{Y_1^v}{Y_2^v}\left\{1 - \exp\left[-Y_2^v\left(I_1(\boldsymbol{\Lambda}^{\mathrm{iso}}) - I_1(\boldsymbol{I})\right)\right]\right\} \\
&\quad + \frac{\kappa_v^{\mathrm{vol}}}{50}\left[\left(I_3(\boldsymbol{\Lambda})\right)^{5/2} + \left(I_3(\boldsymbol{\Lambda})\right)^{-5/2} - 2\right]
\end{aligned}
$$

Time evolutions of loads/reactions

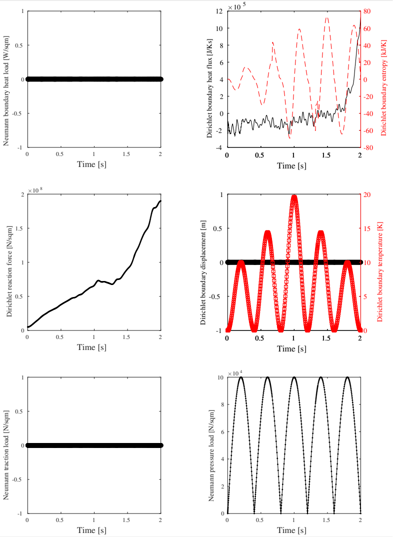

Fiber-reinforced air beam with two cells
(Current configurations (I); $k_{\text{mec}} = 1, k_{\text{the}} = 2, k_{\text{vis}} = 1$)

Motion Status Monitor: Volume dilatation $\det(\tilde{\boldsymbol{F}})$ at $t_n = 1.0$

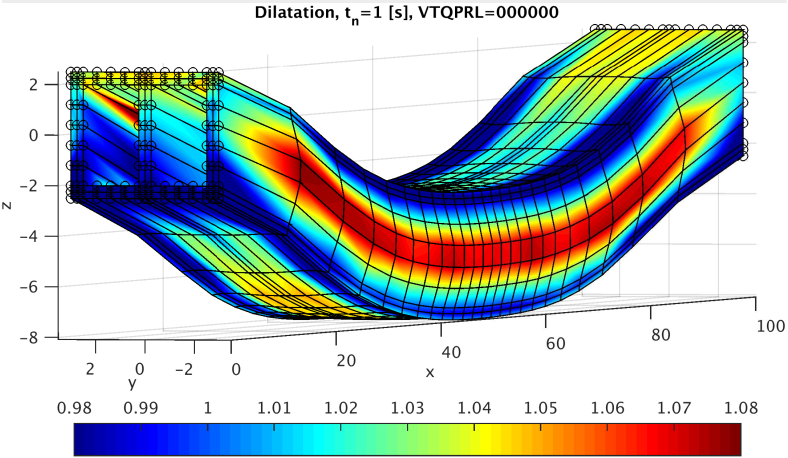

Fiber-reinforced air beam with two cells
(Current configurations (II); $k_{\text{mec}} = 1, k_{\text{the}} = 2, k_{\text{vis}} = 1$)

Motion Status Monitor: Volumetric stress S_V at $t_n = 1.4$

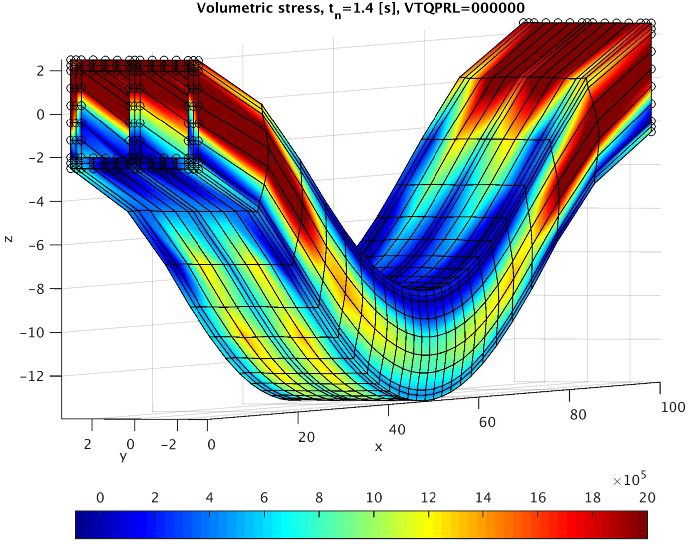

Fiber-reinforced air beam with two cells
(Current configurations (III); $k_{\text{mec}} = 1, k_{\text{the}} = 2, k_{\text{vis}} = 1$)

Motion Status Monitor: Fiber stress S_F at $t_n = 2.0$

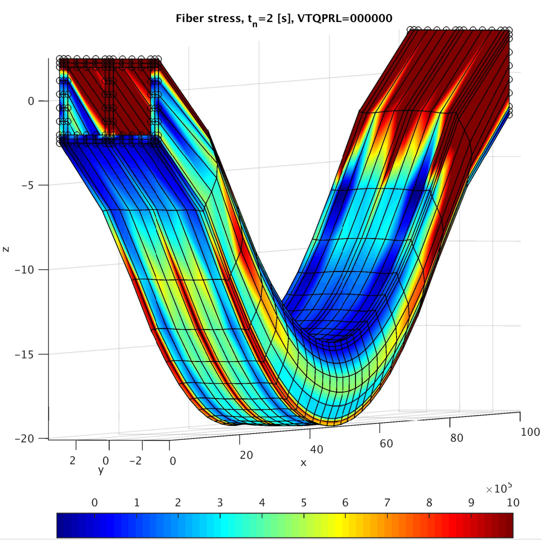

Fiber-reinforced air beam with two cells

(Current configurations (IV); $k_{\text{mec}} = 1, k_{\text{the}} = 2, k_{\text{vis}} = 1$)

Motion Status Monitor: Temperature Θ at $t_n = 1.5$ INSIDE the cell corners

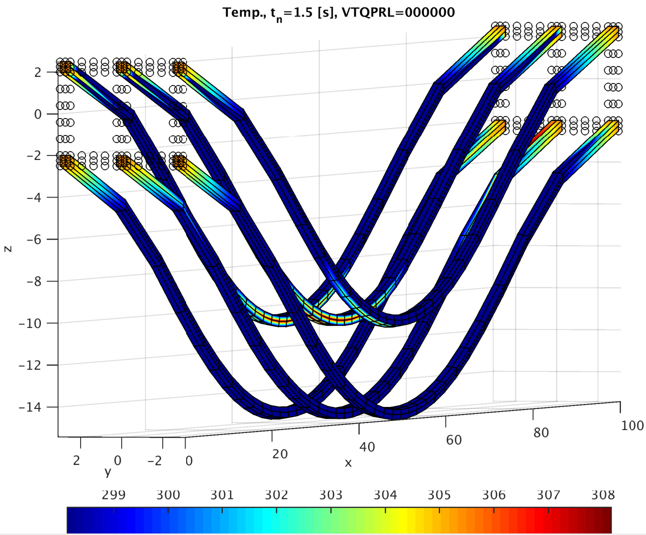

Fiber-reinforced air beam with two cells

(Solutions versus time; $k_{\mathrm{mec}} = 1, k_{\mathrm{the}} = 2, k_{\mathrm{vis}} = 1$)

Fixed node on the boundaries $\partial_{\dot{\Theta}}\mathscr{B}_0$, $\partial_{\varphi}\mathscr{B}_0$

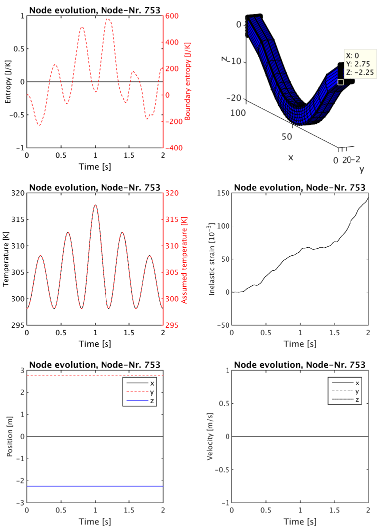

Free node of the middle corner at the center

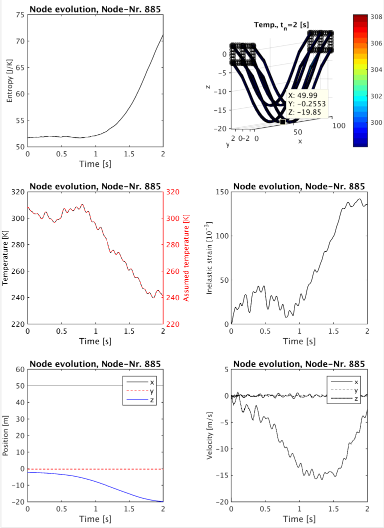

Fiber-reinforced air beam with two cells

(Comparison of $\tilde{N}_B$ (I); $k_{\text{mec}} = 1, k_{\text{the}} = 2, k_{\text{vis}} = 1$)

Current configurations at $t_n = 2.0$: Zoom on bottom surfaces of the beams

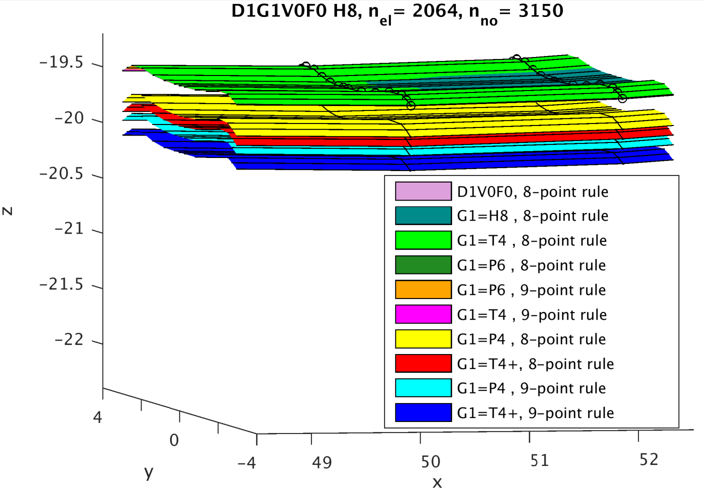

Hourglass functions (cf. Simo, Armero, Taylor [1993])

$$\mathscr{H}_1(\xi,\eta,\zeta) := \xi\,\eta \qquad \mathscr{H}_2(\xi,\eta,\zeta) := \xi\,\zeta \qquad \mathscr{H}_3(\xi,\eta,\zeta) := \eta\,\zeta$$

Fiber-reinforced air beam with two cells
(Comparison of $\tilde{N}_B$ (II); $k_{\text{mec}} = 1, k_{\text{the}} = 2, k_{\text{vis}} = 1$)

Shape functions of $T4+$-$\tilde{\boldsymbol{F}}$-element

$$\tilde{N}_1 = 1 - \xi - \eta - \zeta - \xi\zeta - \eta\zeta - \xi\eta$$

$$\tilde{N}_2 = \xi + \eta\zeta$$

$$\tilde{N}_3 = \eta + \xi\zeta$$

$$\tilde{N}_4 = \zeta + \xi\eta$$

Shape functions of $P4$-$\tilde{\boldsymbol{F}}$-element

$$\tilde{N}_1 = \frac{1}{2}\left[1 - \xi - \eta + \xi\zeta + \eta\zeta\right]$$

$$\tilde{N}_2 = \frac{1}{2}\left[\xi - \xi\zeta\right]$$

$$\tilde{N}_3 = \frac{1}{2}\left[\eta - \eta\zeta\right]$$

$$\tilde{N}_4 = \frac{1}{2}\left[1 + \zeta\right]$$

8-point product Gauss rule

(Felippa [2001], Wriggers [2001])

$l = \sqrt{1/3}, \quad w = 1/(3l^2)$

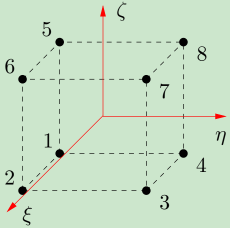

$1 = (-l, -l, -l)$
$2 = (\ \ l, -l, -l)$
$3 = (-l, \ \ l, -l)$
$4 = (\ \ l, \ \ l, -l)$
$5 = (-l, -l, \ \ l)$
$6 = (\ \ l, -l, \ \ l)$
$7 = (-l, \ \ l, \ \ l)$
$8 = (\ \ l, \ \ l, \ \ l)$

9-point non-product Gauss rule

(Simo, Armero, Taylor [1993], Felippa [2001])

$L = \sqrt{3/5} > l, \quad W = 1/(3L^2) < w, \quad W_9 = 8 - 8\,W$

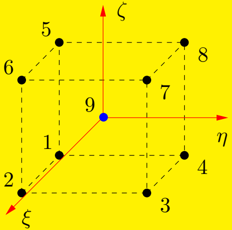

$1 = (-L, -L, -L)$
$2 = (\ \ L, -L, -L)$
$3 = (-L, \ \ L, -L)$
$4 = (\ \ L, \ \ L, -L)$
$5 = (-L, -L, \ \ L)$
$6 = (\ \ L, -L, \ \ L)$
$7 = (-L, \ \ L, \ \ L)$
$8 = (\ \ L, \ \ L, \ \ L)$
$9 = (\ \ 0, \ \ 0, \ \ 0)$

Locking-free higher-order energy-momentum schemes for thermo-viscoelastic fiber-reinforced materials derived by the principle of virtual power

Michael Groß, Julian Dietzsch & Chris Röbiger

Introduction
Variational setting
Continuum model
Variational principle
Discrete setting
Time discretization
Space discretization
Example: H8 mesh
Numerical studies
Numerical example
Configuration and solution
Comparison
Summary

Fiber-reinforced air beam with two cells

(Computational costs; $k_{\text{mec}} = 1, k_{\text{the}} = 2, k_{\text{vis}} = 1$)

Number of time steps / Total cpu time / Number of global iterations

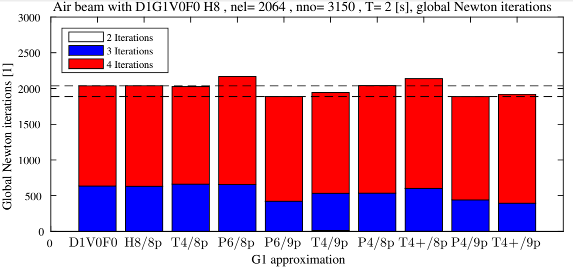

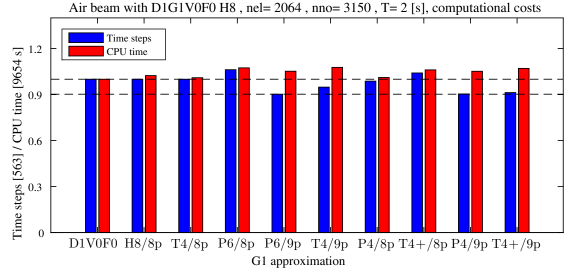

Summary

1. Motivation:
   - Energy-momentum schemes for fiber-reinforced materials
   - related with locking-free meshes for thin-walled structures
2. Goals:
   - Independent space-time approximations
   - of the stretch vector $\boldsymbol{\lambda}_t$ $(\tilde{\boldsymbol{F}})$, and
   - of the volume as well as fiber dilatation $(\tilde{C}_V, \tilde{C}_F)$
3. Strategy:
   - Discretization of a mixed principle of virtual power
   - Design of independent shape functions for spatial derivatives
   - Introduction of appropriate quadrature rules in space
4. Important results:
   - Reduction of locking in meshes of thin-walled structures
   - Increase of maximum time step size due to less artificial stiffness
5. Outlook:
   - Generalization to higher-order hexahedral/tetrahedral meshes

Fiber-reinforced air beam with two cells

(Current configurations (V); $k_{\text{mec}} = 1, k_{\text{the}} = 2, k_{\text{vis}} = 1$)

Motion Status Monitor: Inelastic strain $\|\boldsymbol{C}_i\|$ at $t_n = 1.8$

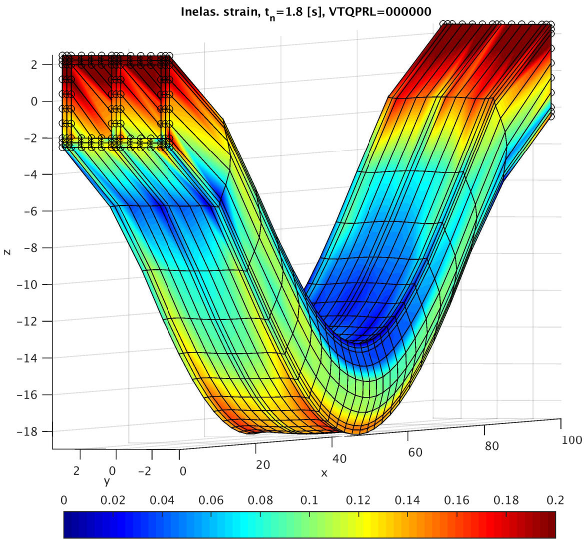

TECHNISCHE UNIVERSITÄT CHEMNITZ

Fiber-reinforced air beam with two cells

(Mechanical/thermal balance laws; $k_{\mathrm{mec}} = 1$, $k_{\mathrm{the}} = 2$, $k_{\mathrm{vis}} = 1$)

Michael Groß, Julian Dietzsch & Chris Röbiger

M-Balance Status Monitor

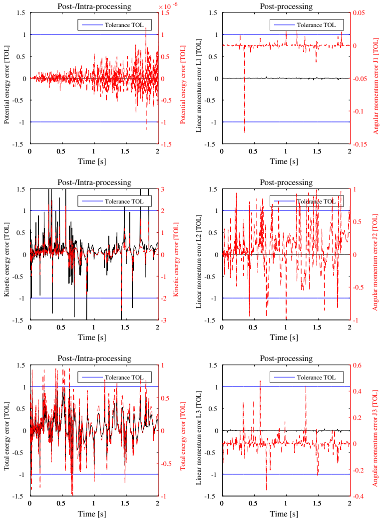

T-Balance Status Monitor

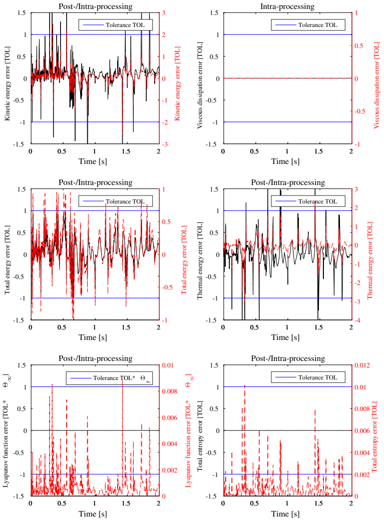

Fiber-reinforced air beam with two cells
(Comparison of $\tilde{N}_B$ (III); $k_{\text{mec}} = 1, k_{\text{the}} = 2, k_{\text{vis}} = 1$)

Time evolutions of reaction force in the clamping (cf. Kasper & Taylor [2004])

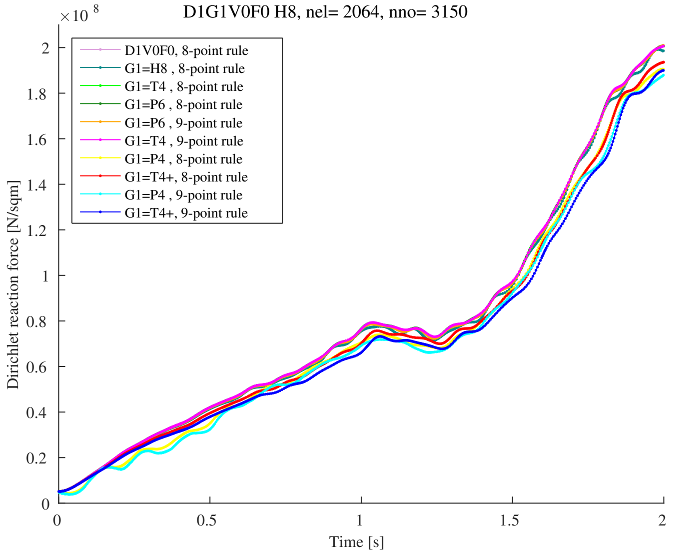

Fiber-reinforced air beam with two cells

(Comparison of $\tilde{N}_B$ (IV); $k_{\text{mec}} = 1, k_{\text{the}} = 2, k_{\text{vis}} = 1$)

Monomials of the H8-derivative (Layers 0,1,2 of Pascal's pyramid)

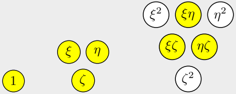

Monomials of the P4 element (Layers 0,1,2 of Pascal's pyramid)

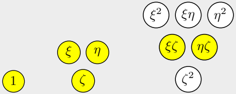

- Missing monomial: $\xi\eta$

Monomials of the T4+ element (Layers 0,1,2 of Pascal's pyramid)

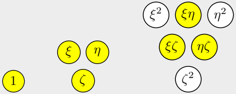

Fiber-reinforced air beam with two cells (H20)
(Comparison of $\tilde{N}_B$ (I); $k_{\text{mec}} = 1$, $k_{\text{the}} = 2$, $k_{\text{vis}} = 1$)

Current configurations at $t_n = 2.0$: Zoom on bottom surfaces of the beams

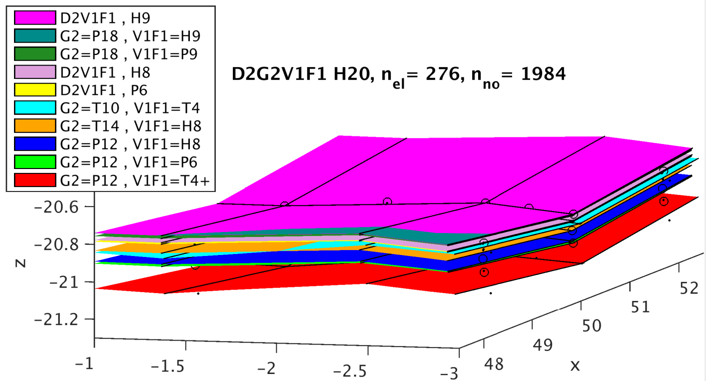

Fiber-reinforced air beam with two cells (H20)
(Comparison of $\tilde{N}_B$ (II); $k_{\text{mec}} = 1, k_{\text{the}} = 2, k_{\text{vis}} = 1$)

Time evolutions of reaction force in the clamping (cf. Kasper & Taylor [2004])

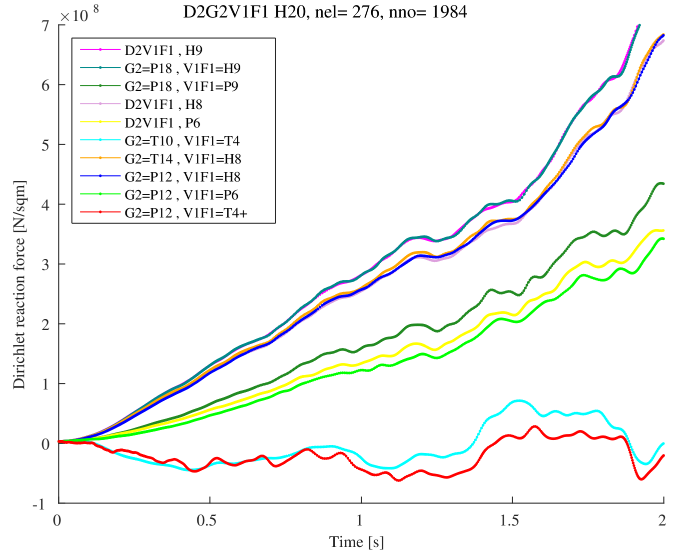

Fiber-reinforced air beam with two cells (H20)
(Comparison of $\tilde{N}_B$ (III); $k_{\text{mec}} = 1$, $k_{\text{the}} = 2$, $k_{\text{vis}} = 1$)

Monomials of the H20-derivative (Layers 0,1,2,3 of Pascal's pyramid)

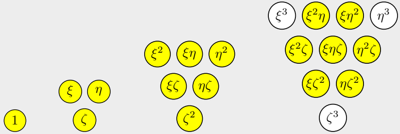

Monomials of the P12 element (Layers 0,1,2,3 of Pascal's pyramid)

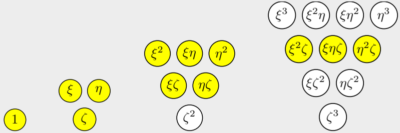

- Missing monomials: ζ^2, $\xi^2\eta$, $\xi\eta^2$, $\xi\zeta^2$, $\eta\zeta^2$

Fiber-reinforced air beam with two cells (H20)
(Comparison of $\tilde{N}_B$ (IV); $k_{\text{mec}} = 1, k_{\text{the}} = 2, k_{\text{vis}} = 1$)

Monomials of the P12-derivative (Layers 0,1,2 of Pascal's pyramid)

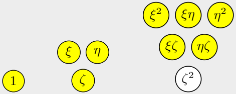

Monomials of the P6 element (Layers 0,1,2 of Pascal's pyramid)

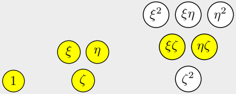

- Missing monomials: ξ^2, $\xi\eta$, η^2

Fiber-reinforced air beam with two cells (H20)

(Computational costs; $k_{\mathrm{mec}} = 1$, $k_{\mathrm{the}} = 2$, $k_{\mathrm{vis}} = 1$)

Number of time steps / Total cpu time / Number of global iterations

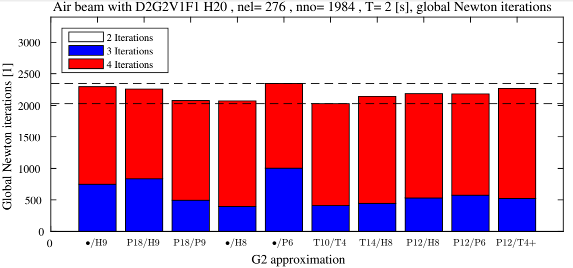

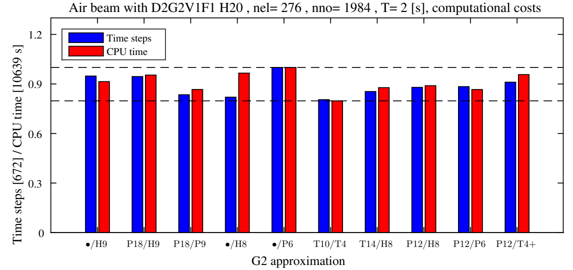

Fiber-reinforced air beam with two cells (H27)
(Comparison of $\tilde{N}_B$ (I); $k_{\text{mec}} = 1, k_{\text{the}} = 2, k_{\text{vis}} = 1$)

Current configurations at $t_n = 2.0$: Zoom on bottom surfaces of the beams

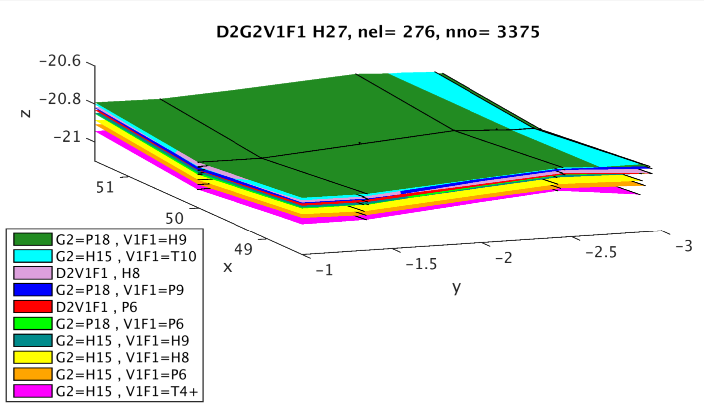

Fiber-reinforced air beam with two cells (H27)

(Comparison of $\tilde{N}_B$ (II); $k_{\text{mec}} = 1$, $k_{\text{the}} = 2$, $k_{\text{vis}} = 1$)

Time evolutions of reaction force in the clamping (cf. Kasper & Taylor [2004])

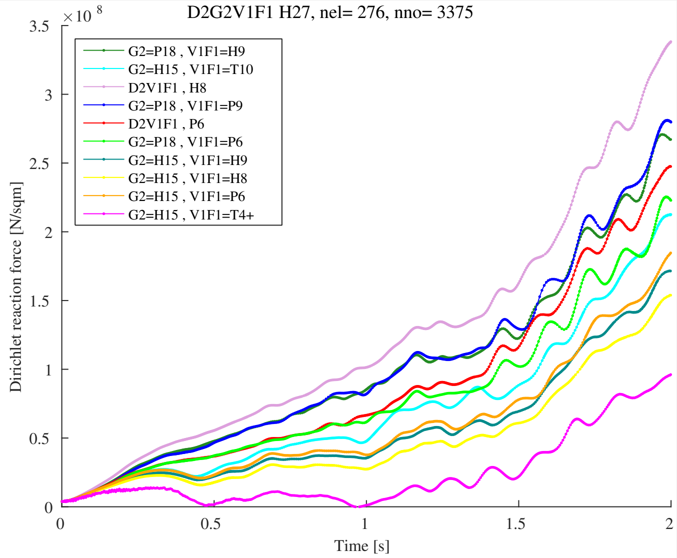

Fiber-reinforced air beam with two cells (H27)

(Comparison of $\tilde{N}_B$ (III); $k_{\text{mec}} = 1$, $k_{\text{the}} = 2$, $k_{\text{vis}} = 1$)

Monomials of the H27-derivative (Layers 0,1,2,3,4,5 of Pascal's pyramid)

1

ξ η ζ

ξ^2 $\xi\eta$ η^2 $\xi\zeta$ $\eta\zeta$ ζ^2

ξ^3 $\xi^2\eta$ $\xi\eta^2$ η^3 $\xi^2\zeta$ $\xi\eta\zeta$ $\eta^2\zeta$ $\xi\zeta^2$ $\eta\zeta^2$ ζ^3

$\xi^3\eta$ $\xi^2\eta^2$ $\xi\eta^3$ $\xi^3\zeta$ $\xi^2\eta\zeta$ $\xi\eta^2\zeta$ $\eta^3\zeta$ $\xi^2\zeta^2$ $\xi\eta\zeta^2$ $\eta^2\zeta^2$ $\xi\zeta^3$ $\eta\zeta^3$

$\xi^3\eta\zeta$ $\xi^2\eta^2\zeta$ $\xi\eta^3\zeta$ $\xi^2\eta\zeta^2$ $\xi\eta^2\zeta^2$ $\xi^2\zeta^3$ $\xi\eta\zeta^3$ $\eta^2\zeta^3$

Monomials of the H15 element (Layers 0,1,2,3,4,5,6 of Pascal's pyramid)

1

ξ η ζ

ξ^2 $\xi\eta$ η^2 $\xi\zeta$ $\eta\zeta$ ζ^2

ξ^3 $\xi^2\eta$ $\xi\eta^2$ η^3 $\xi^2\zeta$ $\xi\eta\zeta$ $\eta^2\zeta$ $\xi\zeta^2$ $\eta\zeta^2$ ζ^3

$\xi^3\eta$ $\xi^2\eta^2$ $\xi\eta^3$ $\xi^3\zeta$ $\xi^2\eta\zeta$ $\xi\eta^2\zeta$ $\eta^3\zeta$ $\xi^2\zeta^2$ $\xi\eta\zeta^2$ $\eta^2\zeta^2$ $\xi\zeta^3$ $\eta\zeta^3$

$\xi^3\eta\zeta$ $\xi^2\eta^2\zeta$ $\xi\eta^3\zeta$ $\xi^2\eta\zeta^2$ $\xi\eta^2\zeta^2$ $\xi^2\zeta^3$ $\xi\eta\zeta^3$ $\eta^2\zeta^3$

$\xi^2\eta^2\zeta^2$ $\xi^2\eta\zeta^3$ $\xi\eta^2\zeta^3$

Fiber-reinforced air beam with two cells (H27)

(Comparison of $\tilde{N}_B$ (IV); $k_{\mathrm{mec}} = 1, k_{\mathrm{the}} = 2, k_{\mathrm{vis}} = 1$)

Monomials of the H15-derivative (Layers 0,1,2,3,4,5 of Pascal's pyramid)

1

ξ η
ζ

ξ^2 $\xi\eta$ η^2
$\xi\zeta$ $\eta\zeta$
ζ^2

ξ^3 $\xi^2\eta$ $\xi\eta^2$ η^3
$\xi^2\zeta$ $\xi\eta\zeta$ $\eta^2\zeta$
$\xi\zeta^2$ $\eta\zeta^2$
ζ^3

$\xi^3\eta$ $\xi^2\eta^2$ $\xi\eta^3$
$\xi^3\zeta$ $\xi^2\eta\zeta$ $\xi\eta^2\zeta$ $\eta^3\zeta$
$\xi^2\zeta^2$ $\xi\eta\zeta^2$ $\eta^2\zeta^2$
$\xi\zeta^3$ $\eta\zeta^3$

$\xi^3\eta\zeta$ $\xi^2\eta^2\zeta$ $\xi\eta^3\zeta$
$\xi^2\eta\zeta^2$ $\xi\eta^2\zeta^2$
$\xi^2\zeta^3$ $\xi\eta\zeta^3$ $\eta^2\zeta^3$

Monomials of the H8 element (Layers 0,1,2,3 of Pascal's pyramid)

1

ξ η
ζ

ξ^2 $\xi\eta$ η^2
$\xi\zeta$ $\eta\zeta$
ζ^2

$\xi^2\eta$ $\xi\eta^2$
$\xi^2\zeta$ $\xi\eta\zeta$ $\eta^2\zeta$
$\xi\zeta^2$ $\eta\zeta^2$

Monomials of the H9 element (Layers 0,1,2,3,4,5,6 of Pascal's pyramid)

1

ξ η
ζ

ξ^2 $\xi\eta$ η^2
$\xi\zeta$ $\eta\zeta$
ζ^2

$\xi^2\eta$ $\xi\eta^2$
$\xi^2\zeta$ $\xi\eta\zeta$ $\eta^2\zeta$
$\xi\zeta^2$ $\eta\zeta^2$

$\xi^3\eta$ $\xi^2\eta^2$ $\xi\eta^3$
$\xi^3\zeta$ $\xi^2\eta\zeta$ $\xi\eta^2\zeta$ $\eta^3\zeta$
$\xi^2\zeta^2$ $\xi\eta\zeta^2$ $\eta^2\zeta^2$
$\xi\zeta^3$ $\eta\zeta^3$

$\xi^3\eta\zeta$ $\xi^2\eta^2\zeta$ $\xi\eta^3\zeta$
$\xi^2\eta\zeta^2$ $\xi\eta^2\zeta^2$
$\xi^2\zeta^3$ $\xi\eta\zeta^3$ $\eta^2\zeta^3$

$\xi^2\eta^2\zeta^2$
$\xi^2\eta\zeta^3$ $\xi\eta^2\zeta^3$

Fiber-reinforced air beam with two cells (H27)

(Computational costs; $k_{\text{mec}} = 1, k_{\text{the}} = 2, k_{\text{vis}} = 1$)

Number of time steps / Total cpu time / Number of global iterations

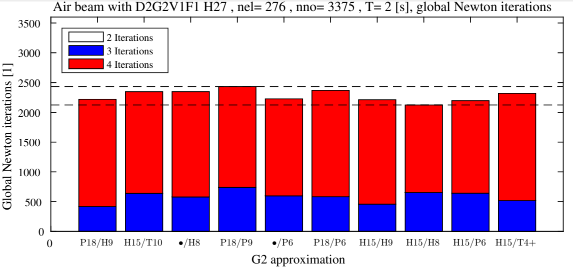

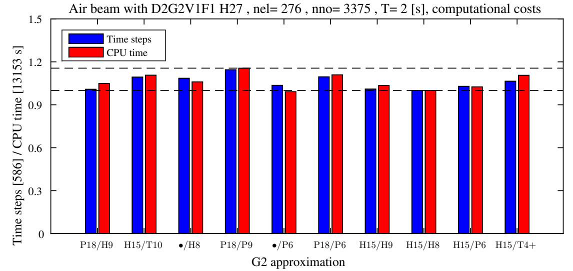

Fiber-reinforced spherical shell with a slit

(Thermodynamical convergence (I); $k_{\text{mec}} = 1, k_{\text{the}} = 2, k_{\text{vis}} = 1$)

Convergence plots

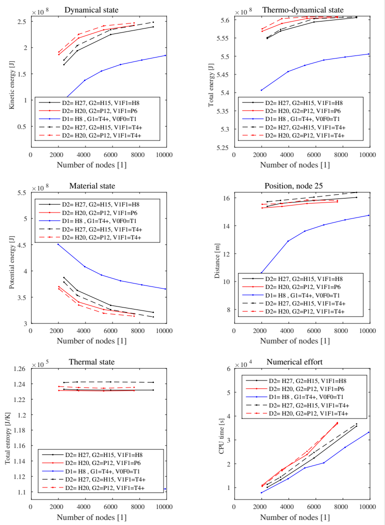

Reaction force, D2G2V1F1 H20

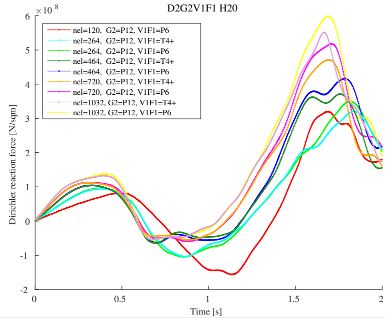

Fiber-reinforced spherical shell with a slit
(Thermodynamical convergence (II); $k_{\mathrm{mec}} = 1, k_{\mathrm{the}} = 2, k_{\mathrm{vis}} = 1$)

Reaction force, D1=H8, G1=T4+, V0F0=T1

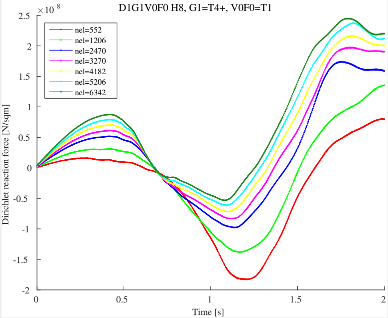

Reaction force, D2G2V1F1 H27